ABSOLUTE INTERFEROMETRIC TEST FOR HIGH NUMERICAL-APERTURE SPHERICAL CONCAVES: GRAVITATIONAL EFFECT

Kenichi HIBINO[1], Ryohei HANAYAMA[2] and Kim YANGJIN[3]

1 National Metrology Institute of Japan, National Institute of Industrial Science and Technology (AIST), Tsukuba, Ibaraki 305-8563, Japan, k.hibino@aist.go.jp
2 The Graduate School for the Creation of New Photonics Industries.
3 The University of Tokyo.

Abstract:

Spherical concaves with high numerical apertures are required in industry for lithography optics in ultraviolet (UV) and X-ray wavelengths. Systematic error in the interferometric test of these surfaces are aberrations due to imperfect alignment, gravitational effect, geometrical effect of nonuniform phase shift, aberrations of converging optics, phase-shift nonlinearity, mechanical vibration, and so on. Gravitational deformation of a 4-inch spherical concave surface was measured in a vertical Fizeau interferometer. Aberrations caused by the deformation was separated and extracted from the total deviations of a sphericity measurement in an absolute test of two spherical comparisons. After subtracting the gravitation deformation from the shape of the spherical concave, we can define a neutral surface which is free from gravity. The gravitational sag in a horizontally placed spherical surface could be measured if we measure the difference of surface shape deviation from this neutral shape. Dominant alignment errors, coma and spherical aberrations were estimated numerically. Experimental results show that the aberrations caused by gravity amount to 7 nm peak-to-valley (PV).

Keywords: Spherical test, Fizeau interferometer, Phase measurement, Gravitational deformation, Phase shift

1. INTRODUCTION

Accurate spherical concaves have been required in industry for commercial interferometers to test aspherical surfaces with high-numerical apertures (NAs), calibration standards in coordinate measuring machines and for lithography and spectroscopy optics in UV and X-ray wavelengths. The typical accuracy necessary for spherical reflective concaves in UV (150 nm wavelength) lithography is, from the Mareshal criterion, equal to λ_{uv} /30 or 5 nm root-mean-squares (RMS). Moreover, the scientists on high energy physics require the surface shape accuracy of better than 1 nm. However, the accuracy of spherical standards available at present commercial interferometers is 15-30 nm. Therefore, spherical surfaces with much better accuracy could be estimated by absolute sphericity measurements.

There are several conventional techniques for absolute testing of spherical surfaces [1]: comparison of two concaves and one convex, comparison of two concaves with three positions, averaging of concave and spherical ball [2], and so on. Among these techniques, three positional measurements for comparing two concave surfaces are most popular because the measurement time is relatively short and the accuracy is as high as $\sim\lambda_{HeNe}$ /120.

The measurement accuracy of the two spherical comparison has been much worse than that of the flatness test (1-10 nm) since there are several additional error sources: the two surfaces cannot be positioned close together while the two centers of the surfaces should be coincided perfectly, the illuminating beam is not a collimated but must be converging, the converging optics has aberrations, and the phase modulation applied by a PZT modulator is spatially non-uniform. One of the ultimate uncertainty occurred in the flatness test is a gravitational deformation (called sag), which usually does not appear in the flatness test literatures [3]. After overcoming the major systematic errors, we can thus expect similar gravitational effect in the spherical test, although the gravitational deformation for small-aperture spherical interferometer has not been reported to the best of our knowledge.

In this experiment, we detected the sag for a 4-inch diameter spherical surface with 48 mm radius of curvature (NA = 0.66) in a vertically placed Fizeau interferometer. The surface deviations of two identical spherical surfaces from the ideal sphere were measured by the absolute test of three positional measurements. The spherical surface was then rotated around the optical axis and the corresponding interference phase was averaged. The gravitational effect was then separated from the other causes of aberrations by the difference of axial symmetry around the optical axis. The centers of curvature of the two sphericals should be spatially coincided to form a confocal position. However, since one of the surfaces was mechanically translated along the optical axis by piezo electric modulator (PZT) and there always exists a misalignment in the initial position of the test surface, the mismatch of the two centers in the lateral and longitudinal directions about the axis caused aberrations. The typical aberrations are third order spherical aberration

and coma aberration. The tolerance of these alignments for obtaining the accuracy of 5 nm is also discussed.

2. GRAVITATIONAL ABERRATION DETECTION IN A SPHERICAL FIZEAU INTERFEROMETER

2.1 Absolute spherical test: Two surface comparison

Commercial Fizeau interferometers are equipped with reference spherical surfaces and compare a test surface with them. The measurement result is the sum of the deviations of the test surface and the reference surface from each ideal sphere surface. A typical accuracy (we call sphericity) of these spherical references is λ/20 or 30 nm peak-to-valley (PV). Therefore, when we like to discuss the surface shape deviation with an accuracy better than 5 nm, we have to determine the surface shape directly by an absolute spherical test.

There have been reported several techniques for the absolute test of spherical surface [2]: comparison of two concave and one convex surfaces, comparison of two concave surfaces in three positions, averaging of a concave surface with a sphere [4]. Here we used the comparison of two concave surfaces in three positions.

Figure 1 shows the three geometries for the two spherical comparisons in a Fizeau interferometer. At least, one of the two spherical surfaces is a transmission type element. In this figure, spherical *A* is a transmission type, which we call transmission sphere. In the first measurement (see Fig. (a)), a plane mirror is located at the focus of the converging lens of the first spherical surface *A* (cat's-eye position). The converging lens is so fabricated that its optical focus is coincident with the center of curvature of the reference surface of spherical *A*. In Fig. 1(a), the reflections from the reference sphere *A* and from the mirror are overlapped to generate interference fringes on an observing screen, placed in front of a charge-coupled device (CCD) detector.

In the second measurement (see Fig. 1(b)), the other spherical surface *B* is located so that its center of curvature is coincident with that of spherical surface *A* (confocal position). The third measurement is similar confocal position, but spherical surface *B* is rotated by 180^{o} around the optical axis.

If we denote the surface deviations from an ideal sphere of the two spherical surfaces by ϕ_A and ϕ_B, and the axially asymmetric component of the aberration of the illuminating beam incident to the surface *A* by ϕ_L, the observed interference phases of the three measurements are given by

$$\varphi_1(x,y)=\frac{2\pi}{\lambda}(\phi_A(x,y)+\phi_A(-x,-y))+\frac{2\pi}{\lambda}(\phi_L(x,y)-\phi_L(-x,-y)), \quad (1)$$

$$\varphi_2(x,y)=\frac{4\pi}{\lambda}(\phi_A(x,y)+\phi_B(-x,y)), \quad (2)$$

$$\varphi_3(x,y)=\frac{4\pi}{\lambda}(\phi_A(x,y)+\phi_B(x,-y)), \quad (3)$$

where λ is the source wavelength, *z*-axis is the optical axis and the *y*-axis is normal to the horizontal plane.

From equations (1)-(3), the deviations of the two spherical surfaces and the aberration of the illumination can be calculated to give

$$\phi_A(x,y)=\frac{\lambda}{8\pi}(\varphi_2(x,y)-\varphi_3(-x,-y))+\frac{\lambda}{8\pi}(\varphi_1(x,y)+\varphi_1(-x,-y)), \quad (4)$$

$$\phi_B(x,y)=\frac{\lambda}{8\pi}(\varphi_2(x,-y)+\varphi_3(-x,y))-\frac{\lambda}{8\pi}(\varphi_1(-x,y)+\varphi_1(x,-y)), \quad (5)$$

and

$$\phi_L(x,y)=\frac{\lambda}{8\pi}(\varphi_1(x,y)-\varphi_1(-x,-y)). \quad (6)$$

Note that in these calculations, spatial tilt and spherical components within each measured phases φ_{1-3} were eliminated before calculating the surface deviations.

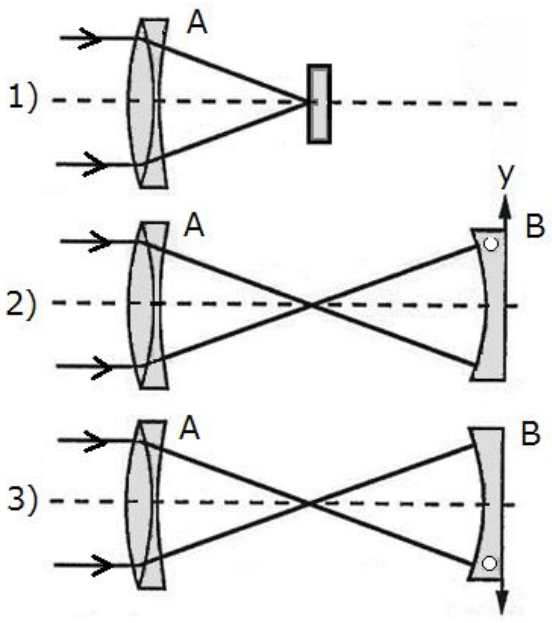

Fig. 1: Optical setup of the three positions for the absolute spherical test. (1) Cat's-Eye position, (2) Confocal position, and (3) Second confocal position. The circular fiducial mark identifies the rotation of surface *B* by 180 degrees around the optical axis.

2.2 Aberration errors in the phase shifting measurement

The measurement accuracy in a spherical test is generally worse than that of a flatness test because there are several additional error sources. The two spherical surfaces cannot be positioned close together, which increases the air

turbulence. Moreover, the centres of curvature of the two spherical surfaces should be positioned strictly together.

During the phase shifting measurement, one of the surface is mechanically translated along the optical axis by 3λ/4 to introduce a phase modulation and thirteen interference images are recorded at equal time interval by a CCD detector. The interference phase calculated by this image is the phase for the middle number of captured images. Since we used 13 images in this experiment, the measured phase is that for the 7th image. The centres of the two surfaces should then coincide when the 7th image is captured. If there is a positional error in the centre of curvature, there occur additional aberrations in the measured phase. Here we estimate the magnitude of these aberrations and discuss the tolerance for the initial alignment error.

First let us discuss a positional error in the lateral direction. Figure 2 shows the ray components that transmit the reference sphere at point *A* and then reflected by the second test surface at point *B*. Points O_1 and *O* are the centres of the reference surface and the test surface, respectively. Since the test surface is strictly not normal to the optical axis, the reflected rays converge to point O_2 different from point O_1. If we denote the vertex of the reference surface by *H* and draw a sphere of radius $O_2H = R$, the rays go across this sphere and the reference surface at points *D* and *E*. Then distance *DE* is the optical path difference between the marginal rays and the axial ray.

The path difference is expanded as to the radial distance r which is the distance from the optical axis as

$$ED = \left\{\left(R - \sqrt{R^2 - (r+\Delta)^2}\right) - \left(R - \sqrt{R^2 - (r-\Delta)^2}\right)\right\} cos\theta$$

$$= \left\{\frac{\Delta r}{R} + \frac{\Delta r^3}{R^3} + \cdots\right\} \cos\theta\,, \tag{7}$$

where Δ is the distance $OO_{1,2}$ and θ is the angle between the ray and the optical axis. The first term in the righthand side of Eq. (7) is a simple tilt component of the test surface, which is not important. The second term is the lowest-order aberration of coma. If we can initially align the test surface and reduce the tilt less component less than λ/80, the first term becomes to

$$\frac{\Delta r}{R} \le \frac{\lambda}{80}. \tag{8}$$

The magnitude of aberration is estimated to be

$$\frac{\Delta r^3}{R^3}\cos\theta \le \frac{\lambda}{80} sin^2\theta\cos\theta = 2.28 \text{ nm}, \tag{9}$$

for numerical aperture of $r/R = \sin\theta = 0.66$ and radius R = 48 mm.

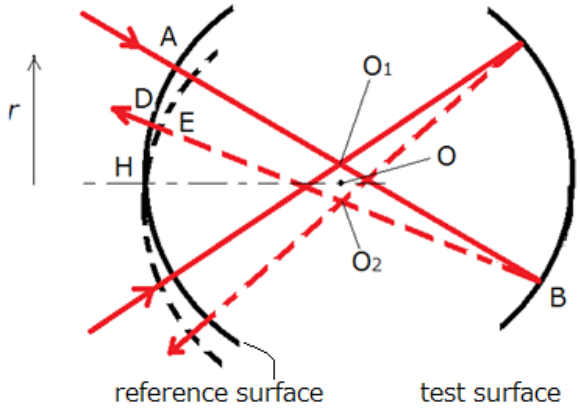

Fig. 2: Wave aberration of a marginal ray when the test surface is slightly inclined to the reference surface normal.

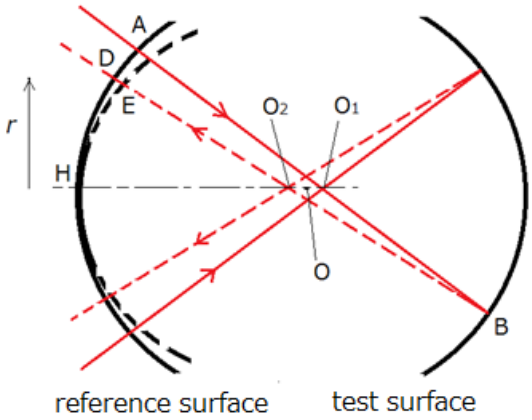

Fig. 3: Wave aberration of a marginal ray when the centre of the test surface is slightly inside the centre of the reference surface.

Secondly we discuss a positional error in the longitudinal direction. Figure 3 shows the ray components. Points O_1 and *O* are the centres of the reference surface and the test surface, respectively, and point O_2 is the converging point of the reflected rays. If we draw a sphere of centre O_2 and radius $O_2H = R_2$, distance *DE* is the optical path difference between the marginal rays and the axial ray. The path difference can be similarly expanded as

$$ED = \left\{\left(R_2 - \sqrt{R_2^2 - r^2}\right) - \left(R - \sqrt{R^2 - r^2}\right)\right\} cos\theta,$$

$$= \left\{\left(\frac{1}{2R_2} - \frac{1}{2R}\right)r^2 + \left(\frac{1}{8R_2^3} - \frac{1}{8R^3}\right)r^4 + \cdots\right\} \cos\theta, \tag{10}$$

where we note $R_2 = R - 2\Delta$ and $R = O_1H$ is the radius of curvature of the reference and the test surfaces.

The first term in the righthand side of Eq. (10) is a residual spherical component of the test surface, which is irrelevant. The second term is the 3rd-order spherical aberration. If we can initially align the test surface and

reduce the longitudinal positional error less than λ/80, the spherical aberration is calculated to give

$$\left(\frac{1}{8R_2^3}-\frac{1}{8R^3}\right)r^4 \le \frac{3}{8}(R-R_2)sin^4\theta cos\theta = 0.62\ nm. \tag{11}$$

From Eqs. (9) and (11), we observe that the dominant wave aberrations caused by a misalignment of the initial position of the test surface and by a positional error of the PZT motion are coma and spherical aberrations. The magnitude of these aberrations is an order of a few nanometer peak-to-valleys in the measured phase.

2.3 Extraction of Gravitational Aberration

Under gravity, a concave surface standing in a vertical plane is expected to deflect about the horizontal axis. For concave spherical surfaces with high numerical apertures, the effect will increase. Here we assume that the two sphericals are identical and undergo the same gravitational deformation which increases the aberration by $\phi_g(x, y)$. We neglect an anisotropic boundary condition that both surfaces are fixed to circular ring mounts, axially symmetric around the optical axis. The surface deviations ϕ_A and ϕ_B in Eqs. (1)-(5) are then replaced by $\phi_A + \phi_g$ and $\phi_B + \phi_g$, respectively.

In addition to the three measurements shown in Fig. 1, we added another measurement in which the test surface *B* in confocal position was rotated around the optical axis stepwise by an equal angle of 30 degrees. The interference phases for twelve positions were averaged. If we denote the rotational average by a upper bar, the measured phase after the average can be described as

$$\bar{\varphi}_4(x,y) = (\phi_A(x,y)+\phi_g(x,y)) + (\bar{\phi}_B(r)+\phi_g(x,y)). \tag{12}$$

We should note that regardless of any rotational position the test surface *B* is always deflected by the gravity in the vertical direction and thus the gravitational component of aberration ϕ_g is not averaged by the rotation.

Substituting ϕ_A in Eq. (4) into Eq. (12), the gravitational aberration is then calculated to give

$$\phi_g(x,y)-\bar{\phi}_g(r) = \bar{\varphi}_4(x,y)+\frac{1}{2}(\varphi_3(-x,-y)-\varphi_2(x,y)) - \frac{1}{2}(\varphi_1(x,y)+\varphi_1(-x,-y)) + (\bar{\phi}_B(r)+\bar{\phi}_g(r)), \tag{13}$$

where the last two terms in the right-hand side give a rotational average of the deviation of the reference surface $\phi_B + \phi_g$ which can be obtained by numerically averaging the right-hand side of Eq. (5) around the optical axis.

2.4 Definition of the Neutral Surface

The second term in the left-hand side of Eq. (13) is an axially symmetric component of the gravitational aberration. In all these calculations, we eliminate the lowest order deviation of tilt and spherical components. Therefore among the deformation by gravity, the lowest order deformation of spherical component is also eliminated from the calculation. We can expect that the asymmetric deformation would be dominant in a vertically standing concave spherical, and the symmetric deformation of the second order (which is proportional to the r^4) be much smaller compared to the asymmetric one.

It will be shown in the next Experiment that the asymmetric component of the gravitational aberration is only an order of several nanometers. We therefore can assume that the symmetric component be zero as

$$\bar{\phi}_g(r) \cong 0, \tag{14}$$

and we calculate the gravitational effect as

$$\phi_g(x,y) = \bar{\varphi}_4(x,y)+\frac{1}{2}(\varphi_3(-x,-y)-\varphi_2(x,y)) - \frac{1}{2}(\varphi_1(x,y)+\varphi_1(-x,-y)) + (\bar{\phi}_B(r)+\bar{\phi}_g(r)). \tag{15}$$

If we subtract the gravitational term ϕ_g from the absolute deviation of the test surface *B*, we can define a neutral shape of the surface A that is free from the gravity effect. The information of neutral surface is useful since the test surface measured absolutely in a vertical interferometer is sometimes used as a reference surface in a horizontally placed interferometer. It is also interesting that we can estimate a gravitational effect for spherical concave surfaces in a horizontally placed Fizeau interferometer. If we compare the surface deviation measured in a horizontal interferometer with its neutral surface shape, we can estimate the magnitude of gravitational aberration in horizontal placement. It is interesting to note that in a flatness test, in contrast, there has not been reported such a neutral surface shape in the absolute test.

3. EXPERIMENTS

Figure 4 shows the optical setup for the phase-shifting Fizeau interferometer. The source beam of He-Ne laser of 633 nm in wavelength is focused to pass through a pinhole and a rotating ground glass diffuser. The beam is then reflected by a polarization beam splitter. The linearly polarized beam is transmitted through a quarter-wave plate to become a circularly polarized beam and is collimated to illuminate the two spherical surfaces *A* and *B* (or a plane mirror in case of the Cats-Eye position). The reflections from both surfaces travel back along the same path, are transmitted through the quarter-wave plate again to attain an

orthogonally linear polarization, pass through the polarization beam splitter, and combine to generate interference fringes on a diffuser screen.

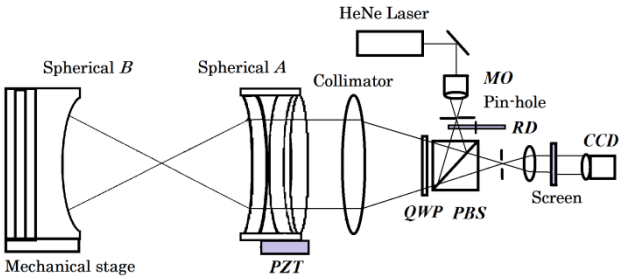

Fig. 4: Optical setup of a spherical test using a Fizeau interferometer, where *MO*, *RD*, *PBS* and *QWP* denote microscope objective, rotating ground glass diffuser, polarization beam splitter and quarter wave plate, respectively.

The interference fringes are recorded by a CCD camera of 640 x 480 pixels from behind the screen.

The samples are two identical transmission spherical surfaces of 4-inch diameter, f /No. = 0.75, and 48.2 mm radius of curvature. All optical components are placed vertically on a optical bench. The temperature within the laboratory was 20.0 degree.

The position of the reference surface *A* is translated by a PZT modulator 12 times with an equal interval of λ/16 and the 13 interference images were recorded in each measurement shown in Fig. 1. The interference phases φ_1, φ_2 and φ_3 were calculated by the phase-shifting algorithm [5] defined by

$$\varphi(x,y) = \arctan \frac{\sum_{r=1}^{13} b_r I_r(x,y)}{\sum_{r=1}^{13} a_r I_r(x,y)}, \tag{16}$$

where the sampling amplitudes are defined by

a_r = (0, -4, -12, -12, 0, 16, 24, 16, 0, -12, -12, -4, 0),

and

b_r = (3, 4, 0, -12, -21, -16, 0, 16, 21, 12, 0, -4, -3). (17)

The random noise mainly caused by mechanical vibration, detector noise and air turbulence degraded the repeatability of the measurement, which gave the repeatability of single phase shifting measurement of typically 4.5 nm rms. The sixty four consecutive measurements were averaged to decrease the random noise to 0.9 nm rms. The surface shapes of the two surfaces ϕ_A and ϕ_B and the aberration of the illuminating beam ϕ_L were calculated by substituting the measured phases into Eqs. (4)-(6).

The test surface *B* was then rotated around the optical axis twelve times in increments of 30 degrees. The interference phases for the twelve angles were averaged. The axial symmetric component of deviation for surface *B* was then calculated numerically. Finally, the gravitational deformation of *B* was calculated using Eq. (13).

If we subtract the gravitational term ϕ_g from the deviation of the test surface *B*. we can define a neutral shape for surface *B* that is free from gravity.

4. RESULTS AND DISCUSSION

Figure 5 (a) and (b) show the measured surface shapes of *A* and *B* after subtracting tilt and spherical components. In order to eliminate the boundary noise region, only 95% of the observing aperture was displayed. The surface deviations from an ideal sphere were 13.3 nm PV and 13.8 nm PV, respectively.

Figure 6 shows the calculated gravitational deformation and its cross-sections along the *x* and *y* axes. The peak observed at the centre of the aperture is noise caused by multiple-surface interference among several surfaces of the converging lenses and the two spherical surfaces, which is common in en-face type Fizeau interferometers. It can be observed from the cross-sections that gravity increases the concavity of the surface by 7 nm in the vertical (along *y*-axis) direction, while it does not affect the surface in the horizontal (along *x*-axis) direction.

We subtract the gravitational term ϕ_g from the deviation of the test surface *B*. Figure 7 shows the calculated neutral surface B which is supposed to be free from gravity effect.

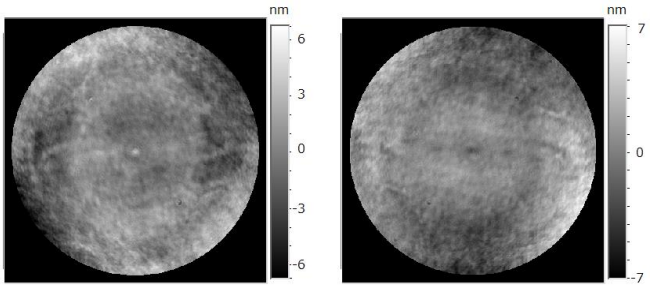

(a) Spherical *A* (b) Spherical *B*

Fig. 5: Measured surface deviaions of the two sphericals of 4-inch diameter, 48.2 mm radius of corvature.

We observed that the surface has a deviation of 22 nm PV that is worse than the original shape of surface *B*.

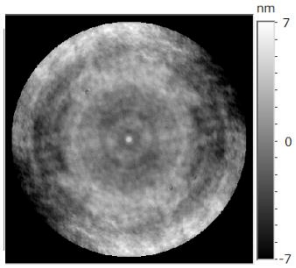

(a) Gravitaional Deformation

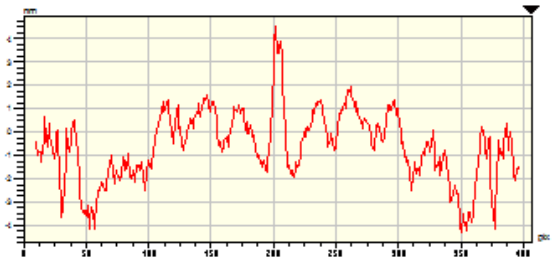

(b) Cross-section along *x*-axis.

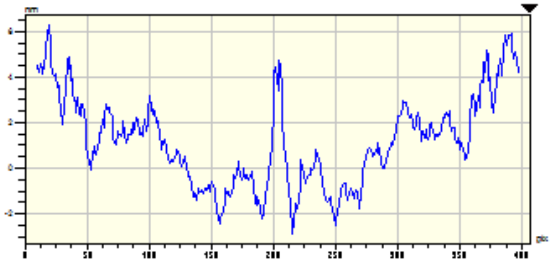

(c) Cross-section along *y*-axis.

Fig. 6: Gravitational aberration of the test spherical surface.

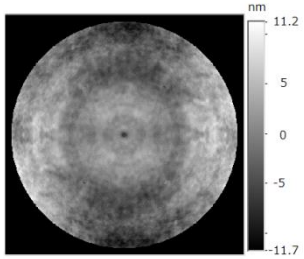

Fig. 7: Neutral surface free from gravity effect.

5. CONCLUSION

Gravitational deformation for spherical concave surface in a vertical Fizeau interferometer was measured. The additional aberration caused by gravity was extracted from the measured surface shape using the different dependency of aberration causes on rotation around the optical axis. The surface shapes of two identical transmission spherical surfaces of 4-inch diameter, 48.2 mm radius of curvature were measured using an absolute spherical test of two-surface comparison with a phase-shifting technique. The dominant aberration caused by an imperfect alignment of the test surface before the phase-shifting were primary coma and spherical aberration. Experimental results showed that the gravitational aberration seems similar to an astigmatism whose magnitude was 7 nm. The aberration is about half the magnitude of the total surface deviation of the spherical surface, which turns out to be significant in the nanometer accuracy measurements.

REFERENCES

[1] J. Burke, ”Rapid and reliable reference sphere calibration for Fizeau interferometry” *Optics Letters* vol. 33(21), pp.2536-2538, 2008.

[2] G. Schultz and J. Schwider, “Interferometric testing of smooth surfaces,” in *Progress in Optics* (North-Holland, Amsterdam) vol.13, pp. 93-167, 1976.

[3] D. Malacara, “Absolute calibration, Phase Shifting Interferometer” in *Optical Shop Testing*, D. Malacara ed. (John Wiley 2007).

[4] J. Burke and Ulf Griesmann, “Calibrating the sag due to gravity of horizontal interferometer reference flats” Proc. of Intererometry XVI: Techniques and Analysis, *SPIE* vol. 8493, pp. 84930F, 2012.

[5] P. de Groot, “Measurement of transparent plates with wavelength-tuned phase-shifting interferometry,” *Appl. Opt.* vol. 39, pp. 2658-2663, 2000.